Temperature dependent TAPO model for failure analysis of adhesive bonds subjected to thermal service loading

Anton Matzenmiller[1], Patrick Kühlmeyer[1]
[1]Institute of Mechanics, Department of Mechanical Engineering, University of Kassel,
Mönchebergstr. 7, 34125 Kassel, Germany

Abstract

The Toughened Adhesive Polymer (TAPO) material model is assigned in LS-DYNA with the keyword ***MAT_252**. The model describes the mechanical behaviour of crash optimised high-strength adhesives under crash conditions and takes elasticity, viscoplasticity and damage due to plastic deformation into account. In this contribution, the TAPO model is extended to temperature dependent viscoelasticity, plasticity and damage considering rate and thermal effects below and beyond the yield strength. Here, the focus of the material model is on failure prediction of joints, which are bonded with ductile-modified adhesives and subjected to service loading with low strain rates due to temperature changes. Therefore, a linear thermo-viscoelastic model is arranged in series to a thermal strain element and the ST.-VENANT body for the TAPO model. The linear viscoelastic material behaviour below the yield strength is represented by the generalised MAXWELL solid with different parallel chains of springs and dashpots describing the equilibrium stress and the overstress. The temperature dependency of the viscosities for the MAXWELL chains is taken into account by the reduced time with the shift function of thermorheologically simple materials. Furthermore, the yield strength and the nonlinear isotropic hardening parameters are empirical functions of temperature. In addition, the damage evolution of the TAPO model is extended with functions of temperature following JOHNSON and COOK as in [1]. By reason of numerical efficiency, the spatial equations of the TAPO model are reduced to the interface theory and implemented into LS-DYNA as a “user defined cohesive model” assuming a thin adhesive layer between the adherends. The parameters of the constitutive equations are identified by fitting the model response to the test data of the Dynamic Mechanical Analysis (DMA), shear tests with the thick adherend shear specimen (TASS) and tension tests with the butt joint specimen (BJS) conducted within the range from ambient temperature to nearly glass transition. Finally, the constitutive equations are validated by means of a test setup with a bimetallic specimen and the Finite Element (FE) Analysis by comparing the model response with the measured test data.

Keywords

thermo-viscoelasticity, thermo-plasticity, damage, cohesive model, ductile-modified adhesive, TAPO

1 Introduction

In modern light weight design, various materials with different physical properties are assembled to large structures, e.g. car bodies or aircraft fuselages. One common joining technology is adhesive bonding, which allows combining a wide range of different materials, e.g. various metals, carbon fibre composites, and polymers. Vastly loaded structures are bonded with high-strength structural adhesives exhibiting high tensile strength and ductility. These properties are achieved by modifying epoxy resin with rubber particles to improve the persistency and energy absorption up to failure by complete fracture. The mechanical behaviour of structural adhesives is generally influenced by deformation, temperature and stress or its rates as well as the degree of polymerisation (cross-linking). The simulation with the Finite Element Method (FEM) is an efficient way to reduce costs in the development process within the framework of computer aided design. Though, constitutive models are necessary for the prediction of the material behaviour under various loading conditions by means of the FE analysis. In this context, the development of phenomenological constitutive models becomes very important for the simulation of adhesively bonded joints.
Recently, the so-called **T**oughened **A**dhesive **Po**lymer (TAPO) model has been made available in LS-DYNA with the keyword **`*MAT_TOUGHENED_ADHESIVE_POLYMER`** (**`*MAT_252`**) for solid elements. The TAPO equations describe the mechanical behaviour of structural adhesives under crash conditions by taking elasticity, viscoplasticity and damage due to plastic deformation into account—see [2], pp. 69-90, [3], pp. 250-282, [4], pp. 54-69, and [5], pp. 2-1152-2-1158. It was developed by the Institute of Mechanics (IfM) at the University of Kassel in both research projects P 676 [2] and P 828 [3]. Also, the TAPO model is applicable for the cohesive elements (**`ELFORM`**=19, 20) in LS-DYNA by means of the option **`*MAT_ADD_COHESIVE`** [5], pp. 2-32—2-34, which reduces the kinematics of the continuum to the local displacement jump, as shown in [3], p. 288, [4], p. 113, and [6]. In addition, the constitutive equations of the TAPO model are reduced to the interface theory for cohesive elements in [4], pp. 106 ff. The interface theory is applied to the failure prediction of adhesively bonded joints with thin adhesive layers in [6] to [9]. Furthermore, the numerical efficiency of cohesive elements is discussed in [9].
As outlined in [2] to [9], the constitutive models are applied to predict failure of bonded structures under crash conditions. Recently, the simulation of adhesively bonded joints focuses also on manufacturing and service processes—see [10] and [11]. Temperature courses influence the material behaviour, important for the design of adhesively bonded structures. Whereas the entire temperature-time history is fundamental for the polymerisation of thermosetting resins. Especially, the thermo-viscoelastic properties of ductile-modified adhesives must be account for in stress levels below and beyond the yield strength.
This contribution concerns with the constitutive modelling of the temperature influence on thermosetting, ductile-modified adhesives, fully cured after polymerisation of the resin. The present investigations focuses on the long-term behaviour of adhesive bonds in bimetallic structures, undergoing temperature induced uneven expansions due to the difference of the thermal expansion coefficients of the adherends. The reduced TAPO model in [4] is extended to temperature dependent viscoelasticity, plasticity and damage with stress exposure beyond the yield strength.
The constitutive model and its consistent tangent modulus are implemented for the quasi-static FE analysis into the code of LS-DYNA to simulate the long-term behaviour of adhesive bonds.
As shown in the validated example, the material model is suited to predict failure of joints subjected to service loading due to evolving temperature courses below the glass transition limit.

2 Thermo-viscoelastic-plastic model with ductile damage

The thin structural adhesive layer of a joint is modelled as an interface between the adherends assuming zero thickness in the model. Hence, an interfacial constitutive model (cohesive zone) is proposed including thermo-viscoelasticity, thermo-plasticity, and ductile damage. The viscoelastic, thermal, and plastic contributions in the model are shown as a serial arrangement of the related bodies in the rheological network in Fig. 1. On the left hand side, the generalised MAXWELL body represents the viscoelastic material properties of the adhesive with different parallel chains of springs and dashpots to describe the overstress response and one parallel spring to account for the equilibrium stress in normal and tangential direction to the interface. The material parameters k_i and g_i are the stiffness of the springs whereas the constants $\hat{\tau}_i^{\mathrm{n,s}}$ are the relaxation times of the MAXWELL chains, while k_∞ and g_∞ are the stiffness parameters for the equilibrium state. The thermal strain element is connected in series to the MAXWELL body in order to describe thermal expansion of the adhesive layer in normal direction:

$$\boldsymbol{\Delta}^{\mathrm{th}} = \tilde{\alpha}_{\mathrm{th}}\, d_{\mathrm{k}} \left(\theta - \theta_0\right) \mathbf{e}_{\mathrm{n}} \;\text{ with }\; \tilde{\alpha}_{\mathrm{th}}{=}2.28 \cdot 10^{-4}\,\mathrm{K}^{-1} \qquad (1)$$

The relative thermal displacement is proportional to the temperature change $\left(\theta - \theta_0\right)$ and the adhesive layer thickness d_{k} with the unit vector normal to the interface $\mathbf{e}_{\mathrm{n}} = \{1 \quad 0 \quad 0\}^{\mathrm{T}}$ and the thermal expansion coefficient $\tilde{\alpha}_{\mathrm{th}}$. So, the thermal element exhibits a thermal displacement jump due to the temperature change only. On the right hand side, the TAPO model is represented by the friction element of ST-VENANT with the yield threshold τ_θ and the spring with the parameters H_θ, q_θ, and b_θ, describing nonlinear isotropic hardening. The rheological network directly provides the additive split of the local, total displacement jump $\boldsymbol{\Delta}$ into a viscoelastic, plastic and thermal contribution:

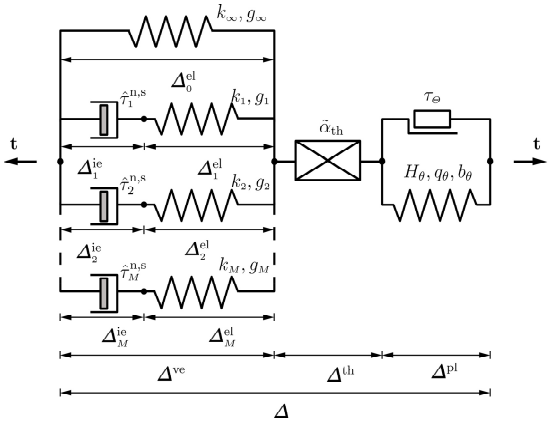

Fig. 1: Rheological network of the interfacial constitutive model

$$\boldsymbol{\Delta} = \boldsymbol{\Delta}^{\mathrm{ve}} + \boldsymbol{\Delta}^{\mathrm{th}} + \boldsymbol{\Delta}^{\mathrm{pl}} \qquad (2)$$

2.1 Thermo-viscoelastic constitutive model

The interface traction $\mathbf{t}$ is postulated as a functional of the viscoelastic displacement jump $\boldsymbol{\Delta}^{\mathrm{ve}}$. Its constitutive parameters are a function of the temperature course $\theta(t)$.

$$\mathbf{t}(t) = \boldsymbol{\mathcal{F}}_{\tau \le t}\left\{\boldsymbol{\Delta}^{\mathrm{ve}}(\tau); \tau, t\right\} \qquad (3)$$

with the time variables t and τ—see [10], p. 177, Eq. (6.4). A thermorheologically simple material behaviour is assumed for the sake of temperature dependent relaxation times—see [12], [13], pp. 266 ff, [14], pp. 202 ff. Due to the time-temperature shift, all relaxation times $\hat{\tau}_i^{\mathrm{n,s}}$ are described with two functions of temperature for the normal (n) and tangential (s) direction of the interface $a_{\mathrm{T}}^{\mathrm{n}}(\theta)$ and $a_{\mathrm{T}}^{\mathrm{s}}(\theta)$. These functions are known as shift functions—see e.g. [15], p. 95. Furthermore, the reduced times ξ_{n} and ξ_{s} are introduced, determined by time integrals of the empirical shift functions

$$\xi_{\mathrm{n}}(t) = \int_0^t \frac{\mathrm{d}s}{a_{\mathrm{T}}^{\mathrm{n}}\left(\theta(s)\right)}\,,\;\; \xi_{\mathrm{s}}(t) = \int_0^t \frac{\mathrm{d}s}{a_{\mathrm{T}}^{\mathrm{s}}\left(\theta(s)\right)}\,, \qquad (4)$$

to take into account the influence of the temperature course $\theta(t)$ on the relaxation times. The time-temperature shift functions consist of an ARRHENIUS-typ equation for temperatures below the reference levels $\theta_{\mathrm{R}}^{\mathrm{n}}$ and $\theta_{\mathrm{R}}^{\mathrm{s}}$ and the WILLIAMS-LANDEL-FERRY equation [16] for temperatures beyond the reference points.

$$a_{\mathrm{T}}^{\mathrm{n,s}}(\theta) = \begin{cases} \exp\left[E_{\mathrm{A}}^{\mathrm{n,s}}\left(\dfrac{1}{\theta} - \dfrac{1}{\theta_{\mathrm{R}}^{\mathrm{n,s}}}\right)\right] & \text{if} \quad \theta < \theta_{\mathrm{R}}^{\mathrm{n,s}} \\ \exp\left[-\dfrac{C_1^{\mathrm{n,s}}\left(\theta - \theta_{\mathrm{R}}^{\mathrm{n,s}}\right)}{C_2^{\mathrm{n,s}} + \theta - \theta_{\mathrm{R}}^{\mathrm{n,s}}}\right] & \text{if} \quad \theta \ge \theta_{\mathrm{R}}^{\mathrm{n,s}} \end{cases} \qquad (5)$$

with the material parameters $E_{\mathrm{A}}^{\mathrm{n,s}}$, $C_1^{\mathrm{n,s}}$, and $C_2^{\mathrm{n,s}}$.

The viscoelastic traction is written as a convolution integral over the viscoelastic displacement jump $\boldsymbol{\Delta}^{\mathrm{ve}}$ with the kernel functions R_{n} and R_{s} in normal and tangential direction of the interface as follows:

$$\mathbf{t} = \int_{-\infty}^{\xi_{\mathrm{n}}(t)} R_{\mathrm{n}}(\xi_{\mathrm{n}}(t) - \tau)\, \frac{\mathrm{d}\Delta_{\mathrm{n}}^{\mathrm{ve}}}{\mathrm{d}\tau}\, \mathrm{d}\tau\; \mathbf{e}_{\mathrm{n}} + \int_{-\infty}^{\xi_{\mathrm{s}}(t)} R_{\mathrm{s}}(\xi_{\mathrm{s}}(t) - \tau)\, \frac{\mathrm{d}\Delta_{\mathrm{t}}^{\mathrm{ve}}}{\mathrm{d}\tau}\, \mathrm{d}\tau\; \mathbf{e}_{\mathrm{t}} + \int_{-\infty}^{\xi_{\mathrm{s}}(t)} R_{\mathrm{s}}(\xi_{\mathrm{s}}(t) - \tau)\, \frac{\mathrm{d}\Delta_{\mathrm{b}}^{\mathrm{ve}}}{\mathrm{d}\tau}\, \mathrm{d}\tau\; \mathbf{e}_{\mathrm{b}} \qquad (6)$$

Both, the traction vector, $\mathbf{t} = \{t_{\mathrm{n}} \quad t_{\mathrm{t}} \quad t_{\mathrm{b}}\}^{\mathrm{T}}$, and the displacement jump vector, $\boldsymbol{\Delta} = \{\Delta_{\mathrm{n}} \quad \Delta_{\mathrm{t}} \quad \Delta_{\mathrm{b}}\}^{\mathrm{T}}$, act in normal, tangential, and binormal direction of the interface. According to [17], p. 60, Eq. (3.3-4), the kernel functions R_{n} and R_{s} are decoupled. From the rheological network of linear springs and NEWTON dashpots, the functions $R_{\mathrm{n}}(t)$ and $R_{\mathrm{s}}(t)$ follow as DIRICHLET-PRONY series for a total of M MAXWELL elements for the normal and each shear component:

$$R_{\mathrm{n}} = k_{\infty} + \sum_{i=1}^{M} k_i \, \exp\left(-\frac{\xi_{\mathrm{n}}(t)}{\hat{\tau}_i^{\mathrm{n}}}\right), \qquad R_{\mathrm{s}} = g_{\infty} + \sum_{i=1}^{M} g_i \, \exp\left(-\frac{\xi_{\mathrm{s}}(t)}{\hat{\tau}_i^{\mathrm{s}}}\right) \tag{7}$$

2.2 Temperature dependent TAPO interface constitutive model

The scalar damage variable D is introduced to describe isotropic damage in the adhesive layer. The definition of damage is based on KACHANOV [18] as the ratio of the damaged to the initial cross section area A_{d} and A_0, respectively—see Fig. 2. It is considered in the equations of the constitutive model by using the concept of effective stress as in RABOTNOV [19]. Here, the nominal traction vector $\mathbf{t}$ in the convolution integral (6) is related to the effective traction vector $\hat{\mathbf{t}}$ according to RABOTNOV's proposal:

$$\hat{\mathbf{t}} = \frac{\mathbf{t}}{1-D} \quad \text{with} \quad D = \frac{A_{\mathrm{d}}}{A_0} \tag{8}$$

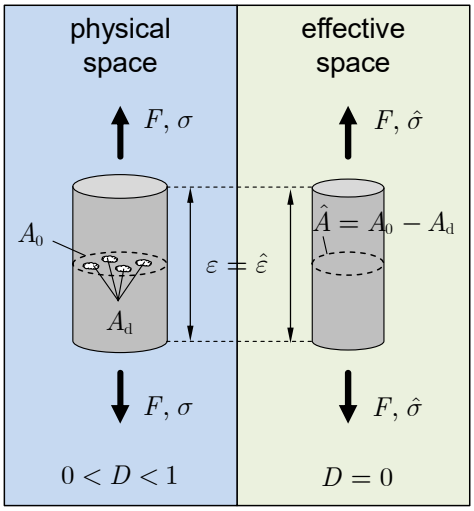

Fig. 2: Motivation of damage and concept of effective stress

In addition, the strain equivalence principle is assumed, which postulates the equality of the strains for the damaged nominal state (physical space) and the undamaged effective state (effective space), $\varepsilon = \hat{\varepsilon}$, see Fig. 2. As a consequence, it leads to the equality of all internal variables of the strain-type, for example $\varepsilon^{\mathrm{pl}} = \hat{\varepsilon}^{\mathrm{pl}}$—see e.g. [20]. In the TAPO cohesive zone model, the interfacial yield function $\tilde{f}$ depends on the normal component $\hat{t}_{\mathrm{n}}$ and the resultant shear stress $\hat{\tau} = \sqrt{\hat{t}_{\mathrm{t}}^{\,2} + \hat{t}_{\mathrm{b}}^{\,2}}$ of the effective interface traction $\hat{\mathbf{t}}$ as well as the yield stress τ_{y} and the yield threshold τ_θ in Eq. $(9)_1$. In addition, the plastic potential $\tilde{f}^*$ $(9)_2$ is presented for a non-associated flow rule to avoid the evolution of the normal plastic displacement jump $\Delta_{\mathrm{n}}^{\mathrm{pl}}$ during a simple shear process.

$$\tilde{f} = \hat{\tau}^2 + \tilde{a}_1 \, \tau_\theta \, \hat{t}_{\mathrm{n}} + \tilde{a}_2 \left\langle \hat{t}_{\mathrm{n}} \right\rangle^2 - \tau_{\mathrm{y}}^{\,2}, \quad \tilde{f}^* = \hat{\tau}^2 + \tilde{a}_2^* \left\langle \hat{t}_{\mathrm{n}} \right\rangle^2 - \tau_{\mathrm{y}}^{\,2} \tag{9}$$

Both functions are defined by using the MACAULEY bracket $\langle x \rangle = (\mathrm{x} + |\,\mathrm{x}\,|)/2$ to obtain asymmetric functions in tension ($\hat{t}_{\mathrm{n}} \geq 0$) and compression ($\hat{t}_{\mathrm{n}} < 0$)—cf. [4], pp. 107 f., Eqs. (7.98), (7.99). In Eqs. (9), the coefficients $\tilde{a}_1$, $\tilde{a}_2$, and $\tilde{a}_2^*$ are constitutive parameters and may depend in principle on temperature change $\theta - \theta_0$:

$$\tilde{a}_2 = \tilde{a}_{20}\left[1 + m_{\mathrm{a2}}\left(\theta - \theta_0\right)\right] \tag{10}$$

with the material parameters $\tilde{a}_{20}$ and m_{a2}. The yield function $\tilde{f}$ and the plastic potential $\tilde{f}^*$ are depicted in Fig. 3—cf. [4], p. 108. Both, the yield function and the plastic potential are elliptic in the first quadrant of the tension-shear-diagram for $\hat{t}_{\mathrm{n}} \geq 0$. If $\hat{t}_{\mathrm{n}} < 0$, the yield function changes into the DRUCKER-PRAGER-like criterion and the plastic potential to the VON MISES-like potential due to the MACAULAY bracket $\langle \hat{t}_{\mathrm{n}} \rangle$ in Eqs. (9)—see second quadrant of the tension-shear-diagram in Fig. 3. The rate of the plastic displacement jump $\dot{\boldsymbol{\Delta}}^{\mathrm{pl}}$ is derived from the plastic potential $(9)_2$ with the effective traction $\hat{\mathbf{t}}$ and the plastic multiplier λ:

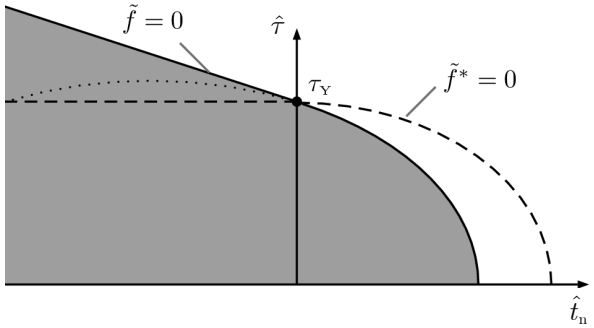

Fig. 3: Yield function $\tilde{f}$ and plastic potential $\tilde{f}^*$ in $\hat{t}_{\mathrm{n}}$-$\hat{\tau}$-diagram at θ_0—cf. [4], p. 108, Fig. 7.16

$$\dot{\boldsymbol{\Delta}}^{\mathrm{pl}} = \lambda \frac{\partial \tilde{f}^{*}}{\partial \hat{\mathbf{t}}} = 2\lambda \left(\tilde{a}_2^{*} \left\langle \hat{t}_{\mathrm{n}} \right\rangle \mathbf{e}_{\mathrm{n}} + \hat{\tau}\, \mathbf{e}_{\tau} \right) \tag{11}$$

The strain equivalence principle leads to non-damaged plastic flow in the effective stress space—cf. [4], p. 108. For the internal variable of the displacement-jump-type, $\dot{r}$ means the plastic arclength given by the EUCLIDean norm of the non-associated flow rule (11):

$$\dot{r} = \sqrt{\dot{\boldsymbol{\Delta}}^{\mathrm{pl}} \cdot \dot{\boldsymbol{\Delta}}^{\mathrm{pl}}} = 2\lambda \sqrt{\left(\tilde{a}_2^{*} \left\langle \hat{t}_{\mathrm{n}} \right\rangle \right)^2 + \hat{\tau}^2} \ , \tag{12}$$

cf. [4], p. 108 f. The yield stress τ_{y} in Eqs. (9) depends on the initial yield threshold τ_θ and the stress of the nonlinear isotropic hardening R, which are both functions of the temperature θ considering the thermal influence on the TAPO plasticity model. Furthermore, the nonlinear isotropic hardening part R is a function of the accumulated plastic arclength r:

$$\begin{aligned} \tau_{\mathrm{y}} &= \tau_\theta(\theta) + R(r,\theta) \text{ with} \\ \tau_\theta &= \frac{\tau_0}{2} \left\{ 1 + \tanh\left[m_\tau \left(\theta_\tau - \theta \right) \right] \right\} \text{and} \\ R(r,\theta) &= q_\theta(\theta) \left[1 - \exp\left(-b_\theta(\theta)\, r \right) \right] + H_\theta(\theta)\, r \end{aligned} \tag{13}$$

The initial yield threshold $(13)_2$ is modelled with a hyperbolic-type function of temperature, defined by means of the constitutive parameters τ_0, m_τ and θ_τ. In contrast to [10] (pp. 203 f.), the parameters in the hardening part q_θ, b_θ, and H_θ follow best hyperbolic tangent functions, which are well defined in the whole range of the absolute temperature $\theta \in [0, \infty)$:

$$\begin{aligned} q_\theta &= \frac{q_0}{2} \left\{ 1 + \tanh\left[m_q \left(\theta_q - \theta \right) \right] \right\} + q_1, \\ b_\theta &= \frac{b_0}{2} \left\{ 1 + \tanh\left[m_b \left(\theta - \theta_b \right) \right] \right\} + b_1, \\ H_\theta &= \frac{h_0}{2} \left\{ 1 + \tanh\left[m_h \left(\theta - \theta_h \right) \right] \right\} + h_1, \end{aligned} \tag{14}$$

with the material parameters q_0, b_0, h_0, m_q, m_b, m_h, θ_q, θ_b and θ_h.

2.3 Temperature dependent damage approach

A ductile damage approach is proposed for the TAPO model to predict damage due to the plastic deformation r, see [3], pp. 267 ff, [4], pp. 60 ff, and [5], p. 2-1157. In this contribution, the damage variable D is driven by the EUCLIDean norm of the vector for the mechanical displacement jump Δ^{vp}:

$$D = \left\langle \frac{\Delta^{\mathrm{vp}} - \Delta^{\mathrm{c}}}{\Delta^{\mathrm{f}} - \Delta^{\mathrm{c}}} \right\rangle^{n_{\mathrm{D}}} \quad , \quad \dot{D} = n_{\mathrm{D}} \left\langle \frac{\Delta^{\mathrm{vp}} - \Delta^{\mathrm{c}}}{\Delta^{\mathrm{f}} - \Delta^{\mathrm{c}}} \right\rangle^{n_{\mathrm{D}}-1} \frac{\dot{\Delta}^{\mathrm{vp}}}{\Delta^{\mathrm{f}} - \Delta^{\mathrm{c}}} \quad \text{with} \tag{15}$$

$$\Delta^{\mathrm{vp}} = \sqrt{\boldsymbol{\Delta}^{\mathrm{vp}} \cdot \boldsymbol{\Delta}^{\mathrm{vp}}} \quad \text{and} \quad \boldsymbol{\Delta}^{\mathrm{vp}} = \boldsymbol{\Delta}^{\mathrm{ve}} + \boldsymbol{\Delta}^{\mathrm{pl}} \ .$$

The damage evolution $(15)_2$ is controlled by the exponent n_{D}, the critical Δ^{c}, and the displacement jump Δ^{f} at failure. In detail, Δ^{c} describes the displacement jump at damage initialisation (tensile strength) and Δ^{f} is the displacement jump at failure of the adhesive in the sense of the approach by JOHNSON and COOK in [1]. Both, Δ^{c} and Δ^{f} are functions of the stress ratio

$$T = \left\langle \hat{t}_{\mathrm{n}} \right\rangle \Big/ \sqrt{\hat{t}_{\mathrm{n}}^{\,2}/3 + \hat{\tau}} \tag{16}$$

according to [4], p. 109. The thermal influence on damage is included by the functions for Δ^{c} and Δ^{f} according to JOHNSON and COOK in [1]:

$$\Delta^{\mathrm{c}} = \left[d_{\mathrm{I1}} + d_{\mathrm{I2}} \exp\left(-d_3 \left\langle T \right\rangle \right) \right] \left[1 - m_{\mathrm{f}} \left(\theta - \theta_0 \right) \right] \ , \ \Delta^{\mathrm{f}} = \left[d_1 + d_2 \exp\left(-d_3 \left\langle T \right\rangle \right) \right] \left[1 - m_{\mathrm{f}} \left(\theta - \theta_0 \right) \right], \tag{17}$$

with the constitutive parameter m_{f}, the room temperature θ_0 at the reference state and d_{I1}, d_{I2}, d_1, d_2, and d_3.

2.4 Implementation

The constitutive equations shown are implemented into the FE software LS-DYNA as a user defined cohesive model for the eight node cohesive zone element (**ELFORM=19,20**)—see [5], pp. 2-264 ff. The thermo-viscoelastic convolution integral is numerically integrated with the recursive, implicit one step algorithm by TAYLOR et al. [21] and solved with the equations of the TAPO plasticity model by a predictor corrector scheme. The consistent tangent modulus is also implemented into LS-DYNA for the quasi-static FE analysis of the long-term behaviour of adhesive bonds.

3 Parameter identification and verification

The parameters of the thermo-viscoelastic model are identified by means of tests with bulk specimens of the adhesive BETAMATE 1496V by DOW Automotive [22] by using the Dynamic Mechanical Analysis (DMA) at the Laboratory for Material and Joining Technology (LWF) at the University of Paderborn. The DMA tests are conducted in the bending and the shear mode to identify the parameters in the DIRICHLET-PRONY series for the elastic $E(t,\theta)$ and shear modulus $G(t,\theta)$ in time t and temperature θ by the time-temperature shift. Here, the elastic parameters $E(t,\theta)$ and $G(t,\theta)$ are approximately used for the interface stiffness in the normal and tangential direction (7) with the layer thickness d_k as follows:

$$R_\mathrm{n}(t,\theta) \approx E(t,\theta)\big/d_\mathrm{k}\ ,\quad R_\mathrm{s}(t,\theta) \approx G(t,\theta)\big/d_\mathrm{k} \tag{18}$$

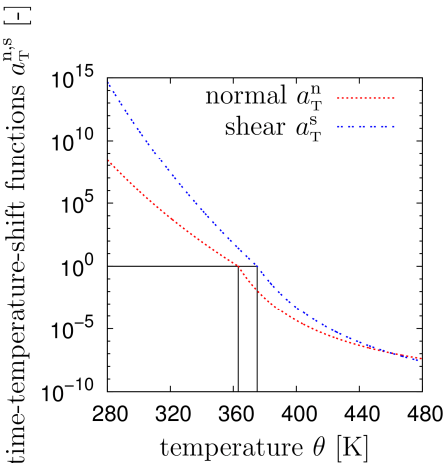

Fig. 4: time-temperature shift functions (LWF)

The time-temperature-shift functions $a_\mathrm{T}^\mathrm{n}(\theta(t))$ and $a_\mathrm{T}^\mathrm{s}(\theta(t))$ are identified empirically at the LWF by shifting the complex moduli of different isothermal temperature states along the frequency axis to obtain a single smooth master curve. Thus, the bending mode provides the data for the time-temperature-shift function for the normal direction and the shear mode comprises the shift function for the tangential direction of the interface—see Eqs. (5). Therefore, the ARRHENIUS and the WILLIAMS-LANDEL-FERRY equation (5) are fitted to the empirical test data of the time-temperature shift along the temperature axis—see courses in Fig. 4.

Tests with the thick adherend shear specimen (TASS) and the butt joint specimen (BJS) are conducted for different constant temperature states at the LWF—see [10], pp. 46-71. The TASS consists of two prismatic steel adherends bonded by an adhesive with constant layer thickness $d_\mathrm{k} = 0.3$ mm and an overlap of 5 mm in the stepped region—see Fig. 5 (a) and [10], p. 13. In the test, the adhesive layer is sheared by moving one of the adherends in the direction tangential to the plane of the adhesive layer with the time-displacement course $\overline{u}_\mathrm{t}(t)$, while the other one is clamped. During the test, the relative displacement between the adherends $\Delta_\mathrm{t}(t)$ is controlled to ensure the nominal shear rate $\tan\dot{\gamma} = \dot{\Delta}_\mathrm{t} \,/\, d_\mathrm{k} = 2.0\cdot10^{-3}\ \mathrm{s}^{-1}$. The resulting force $F_\mathrm{t}(t)$ is measured by a load cell at one of the clamps of the specimen. The test provides the measured data of the relative displacement between the adherends $\Delta_\mathrm{t}(t)$ and the related force $F_\mathrm{t}(t)$. The butt joint specimen consists of two cylindrical, stepped adherends made of steel, which are bluntly bonded by an adhesive with the same layer thickness as defined above—see Fig. 5 (b) and [10], p. 14. Again, one of the adherends is fixed and the other one is displaced normal to the plane of the adhesive layer with the time-displacement course $\overline{u}_\mathrm{n}(t)$. The relative displacement between the adherends $\Delta_\mathrm{n}(t)$ is monitored to force a nominal strain rate of $\dot{\varepsilon} = \dot{\Delta}_\mathrm{n} \,/\, d_\mathrm{k} = 2.0\cdot10^{-3}\ \mathrm{s}^{-1}$ throughout the test.

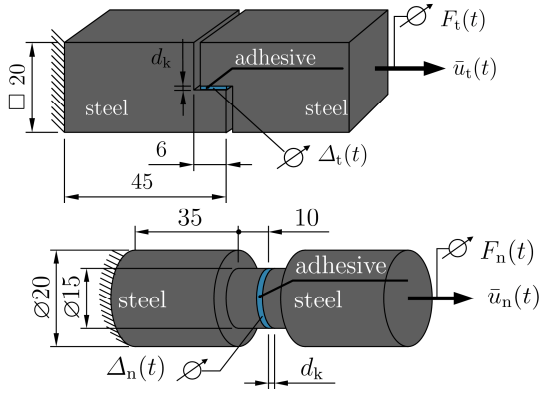

Fig. 5: (a) TASS and (b) BJS with geometrical dimensions in [mm]*, see [10], p. 13-14*

Hence, the test provides the measured data of the relative displacement between the adherends $\Delta_{\mathrm{n}}(\mathrm{t})$ and the related force $F_{\mathrm{n}}(\mathrm{t})$ of the load cell versus time. The FE models take advantage of the symmetry of the specimens in order to reduce the number of elements and nodes—see Fig. 6. In both FE models, the adherends are meshed with solid elements (**ELFORM=2**) and the adhesive layer is modelled with cohesive elements (**ELFORM=19**). For the steel adherends, the isotropic hypoelastic material model (***MAT_001**), suitable for large rotation and small strains, is used with the elastic modulus $E_{\mathrm{st}} = 210000\ \mathrm{N/mm^2}$ and the Poisson ratio $\mu_{\mathrm{st}} = 0.3$—see [5], p. 2-64. The density is set to $\delta_{\mathrm{st}} = 7850\ \mathrm{kg/m^3}$ on the material card. Moreover, the temperature dependent TAPO cohesive model is invoked with the keyword ***MAT_USER_DEFINED_MATERIAL_MODELS** to describe the behaviour of the adhesive bond for the cohesive elements. The adherends of the specimens are connected with the clamps of the tensile testing machine by screws in the test setups. For simplicity, the screws in the adherends are modelled with rigid bodies as shown in the FE models in Fig. 6.

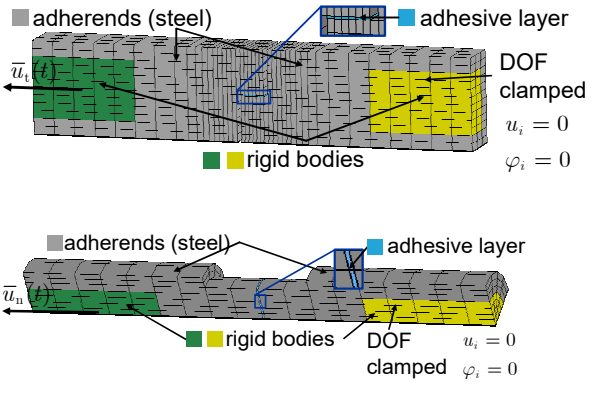

Fig. 6: FE model of the (a) TASS and (b) the BJS with part declaration and boundary conditions

The time-displacement courses of the tests are prescribed for the green rigid bodies with the keyword ***BOUNDARY_PRESCRIBED_MOTION_RIGID**, whereas the yellow rigid bodies are clamped in order to disable all translational u_i and rotational φ_i degrees of freedom (DOF). Also, adequate boundary conditions are prescribed in the symmetry planes of both specimens.

In a second identification step, the instantaneous stiffness parameters $k_0 = k_\infty + \sum_i k_i$ and $g_0 = g_\infty + \sum_i g_i$ of the DIRICHLET-PRONY series are fitted to the first slope of the data in Fig. 7 (a) and (b) measured in the tests with the TASS and BJS to accomplish the stiffness of the adhesive bond. Here, the participation factors $\nu_i^{\mathrm{n}} = k_i/k_0$, $\nu_\infty^{\mathrm{n}} = k_\infty/k_0$ and $\nu_i^{\mathrm{s}} = g_i/g_0$, $\nu_\infty^{\mathrm{s}} = g_\infty/g_0$ are kept constant between the instantaneous stiffness parameters k_0, g_0 and the stiffness parameters of the individual MAXWELL chains k_i, g_i and the equilibrium stiffness k_∞ and g_∞.

Furthermore, the material parameters for the extended TAPO model and the damage approach are inversely identified by fitting the model response of the FE simulation to the related test data of the TASS and the BJS in Fig. 7 (a) and (b)—see [10], pp. 46-71. The result of the identification is added to Fig. 7 comparing the data of the FE result to the test data for the performance of the model in the verification step for different temperature states. It can be observed that the actual yield stress in tension and shear strength steadily decrease with rising temperature, whereas the critical strain at the shear strength increases. In the simulation, the traction is dominated by the overstress in the MAXWELL elements for the quasi-static loading in both test series due to the small equilibrium stiffness k_∞ and g_∞.

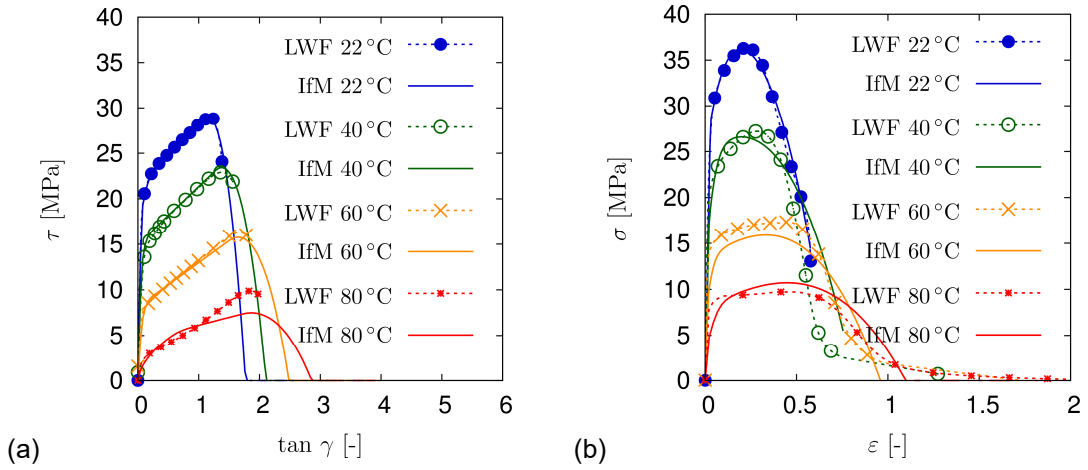

Fig. 7: Comparison of test data from the LWF (dashed lines with symbols) and model response (solid lines) with identified parameters of (a) TASS and (b) BJS

4 Model validation

A bimetallic specimen is tested at the LWF in Paderborn for the purpose of validation—see [10], pp. 237 ff. It consists of an aluminium and a steel sheet strip with different thermal expansion coefficients $\alpha_{\mathrm{al}}^{\mathrm{th}} = 2.4 \cdot 10^{-5}\ \mathrm{K}^{-1}$ and $\alpha_{\mathrm{st}}^{\mathrm{th}} = 1.3 \cdot 10^{-5}\ \mathrm{K}^{-1}$, respectively. For the steel sheet strip, the material parameters are the elastic modulus $E_{\mathrm{st}} = 210000\ \mathrm{N}/\mathrm{mm}^2$ and the Poisson ratio $\mu_{\mathrm{st}} = 0.3$, whereas the parameters of the aluminium strip are taken as $E_{\mathrm{al}} = 70000\ \mathrm{N}/\mathrm{mm}^2$ and $\mu_{\mathrm{al}} = 0.34$. The densities of the steel and aluminium sheet are set to $\delta_{\mathrm{st}} = 7850\,\mathrm{kg}/\mathrm{m}^3$ and $\delta_{\mathrm{al}} = 2700\,\mathrm{kg}/\mathrm{m}^3$. Both strips are joined with the cured, thermosetting, ductile-modified, structural adhesive BETAMATE 1496V at the right hand side and clamped at the left hand side as shown in Fig. 8 (a). The specimen is heated in the oven to achieve a temperature induced thermal expansion of the sheet metals, leading to shear deformations in the adhesive. The bimetallic specimen is tested to investigate the displacement due to bending and shearing of the adhesive under arbitrary thermal loading. The deflection u_z at the tip and the relative displacement between the sheets at the adhesive bond Δu_x are measured with an optical device under a typical time-temperature loading. Therefore, the specimen is linearly heated up from nearly room temperature to about 81 °C within 6 min, followed by a hold time at about 81 °C for 125 min and an uncontrolled cooling process up to nearly room temperature as shown in Fig. 9. Finally, the test data of the bimetallic specimen are compared to the data of the related FE simulation for the validation of the constitutive equations of the temperature dependent TAPO model—cf. [10], pp. 255 ff. The bimetallic specimen is simulated with the FE-program LS-DYNA [23]. In the FE model as in Fig. 8 (b), both sheets are spatially discretised by means of the enhanced solid element (**ELFORM=-2**) and characterised with the isotropic hypoelastic material model ***MAT_001**. The isotropic thermal expansion is taken into account with the keyword ***MAT_ADD_THERMAL_EXPANSION** for both sheets.

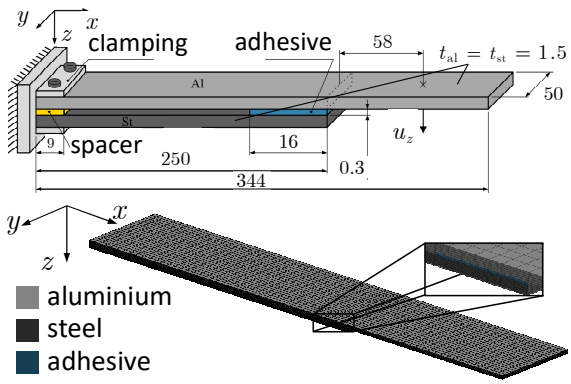

Fig. 8: Bimetallic sheet specimen with (a) dimensions in [mm] *and (b) FE model*—see [10]*, pp. 14 f*

The adhesive is discretised by using the cohesive element (**ELFORM**=19) and is described by the extended TAPO model as user defined. A node to node connection is applied between the cohesive and the solid elements. The representative data of the measured time-temperature-courses of four tests is prescribed to the nodes by means of the load curve using the option ***LOAD_THERMAL_LOAD_CURVE** on the assumption of an approximately homogeneous temperature distribution across the specimen. For simplification, the clamp of the bimetallic specimen is not modelled in detail. Rather, a set of boundary conditions is used to fix the sheets in space and allow thermal expansions at the clamp to prevent artificial stresses in the sheets. In the test setup, a spacer ensures the distance between the sheets at the clamp—see Fig. 8. Therefore, the DOF in z-direction are fixed for the nodes at the bottom of the aluminium and the top of the steel sheet in the area of the clamp. Fig. 10 (a) shows the data of the tip deflection u_z of the four tests in the range from 8 mm to 10 mm at the end of the heating process. During the state of constant temperature, they decrease to approximately 6 mm to 8 mm because of stress relaxation towards the equilibrium stress in the adhesive. Furthermore, u_z declines below its initial value after cooling down to room temperature. In Fig. 10 (b), the test data of the relative displacement Δu_x are plotted versus time t. During the heating process, Δu_x increases to approximately constant values between 0.09 mm and 0.12 mm.

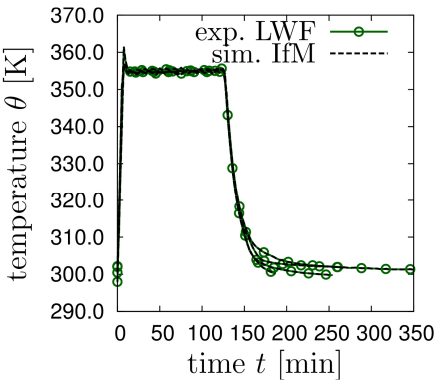

Fig. 9: Time-temperature-course

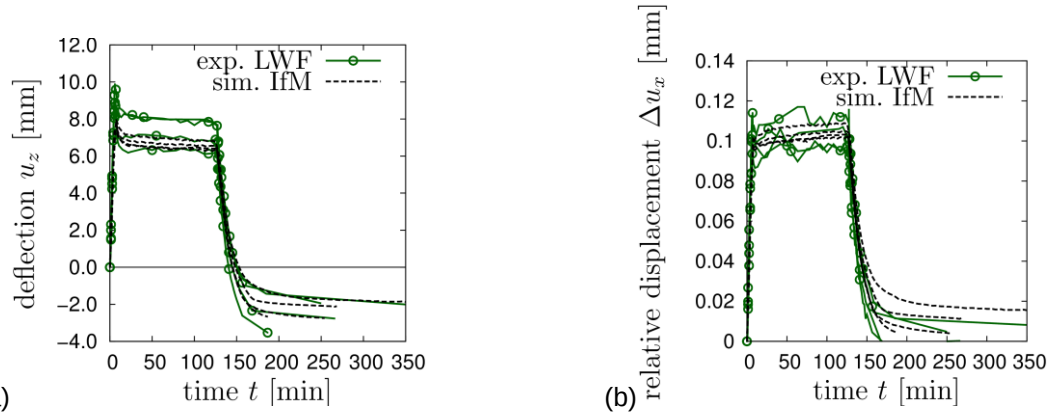

(a) (b)

Fig. 10: Validation of (a) tip deflection u_z and (b) relative displacement Δu_x of bimetal specimen—cf. [10]*, pp. 259 ff*

Finally, the deflection at the tip u_z and the relative displacement Δu_x of the FE simulation are compared to the test data in Fig. 10 (a) and (b). As a result, the computed deflection at the tip u_z is in the range of the scatter band of the measured test data as shown in Fig. 10 (a). In Fig. 10 (b), the relative displacement Δu_x is in a good agreement with the test data, whereas the simulation data of two calculations leave the scatter band of the test data during the cooling process. In the FE simulation, inelastic deformations remain after the cooling process caused by residual inelastic strains in the adhesive as shown in Fig. 10. The interested reader may find the used material parameters in [24].

5 Summary and Outlook

The temperature dependent TAPO model is presented describing thermo-viscoelastic phenomena before and thermo-plasticity beyond the yield threshold. Also, the material model takes temperature dependent damage up to failure into account. The constitutive parameters are identified by fitting the model response of the FE simulation to the related test data of the TASS and the BJS. The constitutive equations are verified by the FE simulation of the tests with the TASS and BJS. Finally, the material model is validated with a bimetallic test by comparing the FE simulation to the measured data in the test. The stress relaxation is indirectly evaluated through the deflection at the tip u_z and the relative displacement between the sheets Δu_x with respect to temperature, deformation, and time by means of the bimetallic specimen. In summary, the constitutive model successfully predicts the test results of the bimetal specimen. Finally, further test have to be performed in order to proof the validity of the proposed constitutive model. In detail, tests are needed exhibiting failure of the adhesive bond during temperature induced deformations of the adherends.

6 Acknowledgement

We thankfully acknowledge financial support of the Federal Ministry for Economic Affairs and Energy through the AiF (Arbeitsgemeinschaft industrieller Forschungsvereinigungen "Otto von Guericke" e.V.) by grant P 878 / 369 ZN of the FOSTA—Forschungsvereinigung Stahlanwendung e.V., Sohnstr. 65, 40237 Düsseldorf, Germany.

7 References

[1] Johnson, G. R., Cook, W. H.: Fracture characteristics of three metals subjected to various strains, strain rates, temperatures and pressures. "EFM", vol. 21, pp. 31-48, 1985.

[2] Schlimmer, M., Barthel, C., Pauli, J., Siebert, M., Matzenmiller, A., Fiolka, M., Gerlach, S., Mahnken, R., Hentrich, M., Hahn, O., Jendrny, J., Wißling, M., Dilger, K., Welters, T., Gumbsch, P., Andrieux, F., Memhard, D., Sun, D.-Z., Thoma, K., Nossek, M., Sauer, M., Hennemann, O.-D., Brede, M. (ed.), Hesebeck, O. and Marzi, S.: "Forschung für die Praxis P 676: Development of Methods to Simulate High Strength Adhesive Joints with Sheet Steel at Crash Conditions for Vehicle Construction". Report of project P 676, FOSTA e. V., Sohnstraße 65, 40237 Düsseldorf: Verlag und Vertriebsgesellschaft mbH, Düsseldorf, 2008. Download author-created version.

[3] Brede, M., Hesebeck, O. (eds.), Marzi, S., Mahnken, R., Nörenberg, N., May, M., Kilchert, S., Voß, H., Matzenmiller, A., Burbulla, F., Memhard, D., Böhme, W., Lienhard, J., Fehrenbach, C. and Reissig, L.: "Robustness and Reliability of Methods to Simulate Adhesive Joints with High Strength Steel Sheets at Crash Conditions". Report of project P 828, Forschungsvereinigung

Stahlanwendung e. V., Sohnstr. 65, 40237 Düsseldorf, in press. Download author-created version.

[4] Burbulla, F.: "Kontinuumsmechanische und bruchmechanische Modelle für Werkstoffverbunde", PhD thesis, Institute of Mechanics, Department of Mechanical Engineering, University of Kassel, 2015.

[5] Livermore Software Technology Corporation (LSTC): LS-DYNA keyword user´s manual – volume II – Material Models – 03/23/15. Livermore, California, USA, 2015.

[6] Matzenmiller, A. and Burbulla, F.: "Kontinuumsmechanische Modellierung von Stahlblechklebverbindungen für die FE-Crashanalyse", Proceedings of the 7th LS-DYNA Forum, 2008, Bamberg, DYNAmore GmbH, Stuttgart, 2008. [PDF]

[7] Gerlach, S., Fiolka, M. and Matzenmiller, A.: "Modelling and analysis of adhesively bonded joints with interface elements for crash analysis", Proceedings of the 4th LS-DYNA Forum, 2005, Bamberg, DYNAmore GmbH, Stuttgart, 2005. [PDF]

[8] Matzenmiller, A., Gerlach, S. and Fiolka, M.: "Progressive Failure Analysis of Adhesively Bonded Joints in Crash Simulations", Proceedings of the 5th LS-DYNA Forum, 2006, Ulm, DYNAmore GmbH, Stuttgart, 2006. [PDF]

[9] Matzenmiller, A., Gerlach, S. and Fiolka, M.: A critical analysis of interface constitutive models for the simulation of delamination in composites and failure of adhesive bonds. "Journal of Mechanics of Materials and Structures", vol. 5 (2), pp. 185-211, 2010.

[10] Meschut, G., Teutenberg, D. (ed.), Lion, A., Liebl, C., Matzenmiller, A. and Kühlmeyer, P. (ed.): "Development of Methods for Simulation and Evaluation of Damage in Adhesive Layers due to Thermal Cyclic Loadings during Manufacturing and Operation". Report of project P 878, Forschungsvereinigung Stahlanwendung e. V., Sohnstr. 65, 40237 Düsseldorf, in press. Download author-created version.

[11] Liebl, C.: "Viskoelastisch-viskoplastische Modellierung von Strukturklebstoffen während der Aushärtung", PhD thesis, Institute of Mechanics, Faculty of Aerospace Engineering, Munich University of the Federal Armed Forces, 2014.

[12] Schwarzl, F. R., Staverman, A.J.: Time-Temperature Dependence of Linear Viscoelastic Behavior. "Journal of Applied Physics", 23(8), 838–843, 1952.

[13] Ferry, J.D.: "Viscoelastic Properties of Polymers", John Wiley & Sons, 3rd Edition, 1980.

[14] Schwarzl, F. R.: "Polymermechanik, Struktur und mechanisches Verhalten von Polymeren", Springer-Verlag, 1990.

[15] Christensen, R. M.: "Theory of Viscoelasticity, An Introduction", Academic Press, 1982.

[16] Williams, M. L. ,Landel, R. F. and Ferry, J. D.: The Temperature Dependence of Relaxation Mechanisms in Amorphous Polymers and Other Glassforming liquids. "Journal of the American Chemical Society", 77(14), S. 3701–3707, 1955.

[17] Matzenmiller, A., Kurnatowski, B., Hanselka, H., Bruder, T., Schmidt, H., Mayer, B., Schneider, B., Kehlenbeck, H., Nagel, C. and Brede, M. (ed.): "Design of Adhesive Joints with Steel Components at Loading with Variable Amplitudes for Vehicle Construction". Report of project P 796, FOSTA e. V., Sohnstr. 65, 40237 Düsseldorf, 2012. Download author-created version.

[18] Kachanov, L. M.: Rupture time under creep conditions. "International Journal of Fracture", vol. 97, pp. 11-18, 1999. Translated from Izvestia Akademii Nauk SSSR, Otdelenie tekhnicheskich nauk, vol. 8, pp. 26-31, 1958, in Russian.

[19] Rabotnov, Y. N.: On the equations of state of creep. "Proceedings of the Institution of Mechanical Engineers", Conference Proceedings, vol. 178, pp. 2-117-2-112, 1963.

[20] Bröcker, C. and Matzenmiller, A.: Thermomechanically consistent material modeling with damage for simultaneous hot/cold forming based on enhanced rheological models. J. Eberhardsteiner, H. Böhm and F. Rammerstorfer (eds.): "Proc. of 6th European Congress on Computational Methods in Applied Sciences and Engineering (ECCOMAS)". Vienna Universtity of Technology, Austria, 2012.

[21] Taylor, R. L., Pister, K. S., Goudreau, G. L.: Thermomechanical analysis of viscoelastic solids. "International Journal for Numerical Methods in Engineering", vol. 2, pp. 45-59, 1970.

[22] Dow Automotive: Techincal Datasheet BETAMATE 1496 V. Issue 10, 04.06.2007. Dow Automotive (Deutschland) GmbH, 65824 Schwalbach, 2007.

[23] Livermore Software Technology Corporation (LSTC): LS-DYNA keyword user´s manual – vol. I – 03/23/15. Livermore, California, USA, 2015.

[24] Kühlmeyer, P., Matzenmiller, A.: Temperature dependent TAPO model for failure analysis of adhesively bonded joints due to temperature induced manufacturing and service loading. "7. Doktorandenseminar Klebtechnik", September 29 – 30, 2016, Wolfsburg. DVS-Berichte: DVS Media GmbH, in press. Download author-created version.